based on M/G/1 with a HOL-NPR (head-of-line non-pre-emptive) queueing model. We define a new concept of trunk as a group of voice traffic with identical destination and DSCP. It is assumed that at least one trunk should be established between the ingress router and corresponding egress router. Each trunk has a different voice traffic arrival rate and mean service time. We assume that there are P types of queues. In a queue of type k (k = 1, 2, ..., P), there are m_k servers and no waiting room.

Packet loss occurs in two ways. In one, a packet arrives when its trunk is full; in the other, the trunk is empty but the reservation at the second step fails on arrival. We denote the blocking probability of packets arriving in trunks of type k in the former and the latter cases by $P_{loss}^{(1)}(k)$ and $P_{loss}^{(2)}$, respectively. $P_{loss}^{(1)}(k) \cdot \rho_k = \lambda_k h_k$ denotes the traffic intensity in a trunk of type k.

$$P_{loss}^{(1)}(k) = \frac{U_k(N, C(ml))}{N_k} \frac{B(m_k, \rho_k)}{1 - P_k(0)} \quad (1)$$

where $B(m, \rho)$ denotes the blocking probability with traffic intensity ρ. It is well known that $B(m, \rho)$ can be computed by the recursion [3];

$$B(m, \rho) = \frac{\rho B(m-1, \rho)}{m + \rho B(m-1, \rho)} \qquad m = 1, 2, \ldots \quad (2)$$

Next we consider the overall blocking probability $P_{loss}(k)$. Since the blocking probability is the fraction of lost customers to customers arriving in a unit time, we have

$$P_{loss}(k) = 1 - \frac{M_k U_k(N, C(ml))}{N_k \rho_k}$$

$$\text{where} \quad M_k = \frac{\sum_{i=1}^{m_k} i P_k(i)}{1 - P_k(0)} = \frac{\rho_k (1 - B(m_k, \rho_k))}{1 - P_k(0)} \quad (3)$$

However, the above blocking probability is effective in the case of the total waiting time for customers from type k in which class N cannot exceed the end-to-end delay bounds. The total waiting time T_p in our queueing model is defined as follows:

$$T_p = \frac{h_k(1 - \sigma_k) + \sum_{i=1}^{m_k} \lambda_k h_k^2 / 2}{(1 - \sigma_k)(1 - \sigma_{k+1})} \quad \text{where} \quad \sigma_k = \sum_{i=1}^{m_k} \rho_k \quad (4)$$

Results: We have evaluated the blocking probability using our proposed scheme. We treat the heterogeneous trunk case and assume two types of traffic, high and low. High traffic flows are preferentially assigned to the DSCP_EF trunks. High trunks have a larger capacity than low trunks, in order to meet their higher demand. The low traffic flows are assigned to the DSCP_AF and DSCP_BE trunks according to the trunk conditions. In our evaluation, the total amount of traffic is fixed to 12700 flows. Therefore, the mean utilisation becomes 84.7% if there is no blocking.

Table 1: Voice traffic blocking probability

M_L	$P_{loss}(H)$	$P_{loss}(L)$
2	10^{-6}	0.798
4	10^{-6}	0.1
6	10^{-6}	0.098
8	10^{-6}	0.001
10	10^{-6}	0.0000429
12	10^{-6}	0.096
14	10^{-6}	0.1098
16	10^{-6}	0.689

Table 1 shows the voice traffic blocking probability according to the varying capacity of each low class trunk. In this case, the amount of DSCP_EF is fixed at 1400 flows. From Table 1, the optimal value for minimising the voice traffic blocking probability for DSCP_AF and DSCP_BE trunks exists in which DSCP_EF, DSCP_AF, and DSCP_BE trunk blocking probability become < 10^{-4}. It shows that the QoS requirements are well satisfied by using our proposed scheme. Additionally, the same results are obtained when the capacity of each of the high-class trunks varies with time.

Conclusions: We have presented a voice traffic multiplexing scheme with guaranteed QoS between VoIP access routers using differentiated services (DiffServ). At the ingress router, the newly defined RTP/UDP/IP packets, namely, the *L_packet* (long packet), are multiplexed for transmission efficiency by grouping the packets with identical destination egress routers and DSCP. To validate the proposed scheme, a network model has been developed to analyse the blocking performance. Additionally, we have analysed the model using M/G/1 with an HOL-NPR queueing system. Finally, we have presented the numerical results of the analysis. Through the results, the proposed scheme is shown to be very efficient at guaranteeing the QoS requirements over VoIP.

24 November 2000
Electronics Letters Online No: 20010555
DOI: 10.1049/el:20010555

E.J. Ha and J.T. Park (*Department of Electronic Engineering, Kyungpook National University, 1370 SanKyug-Dong, Buk-Gu, Taegu, Korea*)

E-mail: park@ee.knu.ac.kr

References

1 IIDA, K., TAKINE, T., SUNAHARA, H., and OIE, Y.: 'Delay analysis for CBR traffic in static-priority scheduling: single-node and homogeneous CBR traffic case'. IEEE SPIE'97, 1997
2 HOSHI, T., TANIWAQA, K., and TSUKADA, K.: 'Voice stream multiplexing between IP telephony gateways', *IEICE Trans. Inf. Syst.*, 1999, **E82-D**, (4)
3 ROSS, K.W.: 'Multiservice loss models for broadband telecommunication networks' (Springer, Berlin, 1995)

Ion-exchanged waveguide add/drop filter

D.F. Geraghty, D. Provenzano, M. Morrell, S. Honkanen, A. Yariv and N. Peyghambarian

An add/drop filter is fabricated using ion-exchanged waveguides and photowritten Bragg gratings. The device exhibits 20 dB extinction ratios and 3 dB bandwidths of 0.4 nm (100 GHz).

Extensive work has been done on the development of add/drop filters due to their functionality in all-optical networks. Ion-exchanged waveguides have demonstrated low propagation loss [1], negligible birefringence [2] and photosensitivity [3]. Numerous devices have been fabricated using this technology [1].

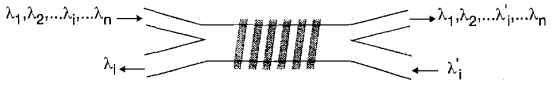

639/1

Fig. 1 *Schematic diagram of grating-assisted wavelength channel add/drop filter*

Here we report the demonstration of an add/drop filter using ion-exchanged waveguides and photowritten Bragg gratings. The device design is similar to previously reported ones that used fibre [4] and silica-on-silicon [5] waveguide technology. A schematic diagram is shown in Fig. 1. Two singlemode waveguides of different widths are brought together into a two-mode section. The two-mode section is again later separated into the two singlemode waveguides. Input signals on the narrow waveguide are coupled to the odd mode of the two-mode section. A tilted grating breaks the orthogonality of the two modes and reflects one wavelength channel to the backwards propagating even mode, and back out the wide 'drop' port. The rest of the channels continue on to the output port. Additionally, a signal at the dropped wavelength can be added through the fourth port.

Surface waveguides were formed in borosilicate glass by silver ion-exchange [1]. The waveguides were formed by first patterning a 100 nm thick Ti mask layer on the glass substrate with the add/drop design. The Ti mask was oxidised for 1 h in an $NaNO_3$ salt melt at 380°C. The sample was then placed into an $AgNO_3$ salt

melt at 300°C for 15 min. The Ti mask was removed and the waveguides were buried for 5 min with a voltage of 310 V. Finally, the sample was cut and the end facets were polished. Modelling predicts that for the chosen ion-exchange times, waveguides with 2–4 μm mask openings will be singlemode and waveguides with 5–7 μm mask openings will be two-mode. The device was designed to have input/output singlemode waveguides widths of 2.5 and 3.5 μm, and a two-mode section width of 6 μm.

Bragg gratings were photowritten over the two-mode section of the devices. A phase mask was chosen to give a periodicity of 535 nm. An area 8 × 2 mm was exposed for 12 min with 85 mJ per pulse and a pulse repetition rate of 50 Hz. The gratings were intended to be written at an angle of 3°, however difficulty in alignment leads to a margin of error of ±0.5°.

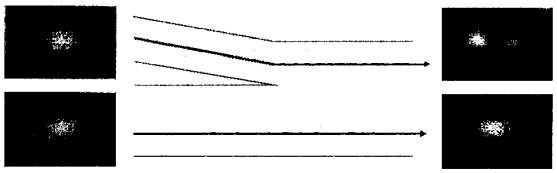

639/2

Fig. 2 *Mode pictures showing operation of input asymmetric y-branch*

The first step in characterising the performance was to assess if the asymmetric y-branches were operating as intended: the mode from the wider input guide gets coupled to the even mode of the two-mode guide and the mode from the narrower guide gets coupled to the odd mode of the two-mode guide. Fig. 2 shows mode pictures from a device without Bragg gratings. The input asymmetric y-branch works nicely, however it is clear that the narrow input does not excite the odd mode perfectly. This is most likely due to imperfections in the photolithography, causing coupling between the two modes. This leads to some coupling to the wide waveguide output. This coupling was measured to be less than 6%: acceptable for this demonstration but too much for system level operation of a device.

Both the transmission and reflection (out of the 'drop' port) of the device were characterised using a tunable laser. A polarisation controller allowed characterisation of both the TE and TM performance. A polariser was used at the output to ensure separation of the polarisations in transmission. It was also used to guarantee that the orthogonal polarisation was down by at least 20 dB for the reflection measurements where we were unable to use a polariser. These measurements were done for both inputs to the device.

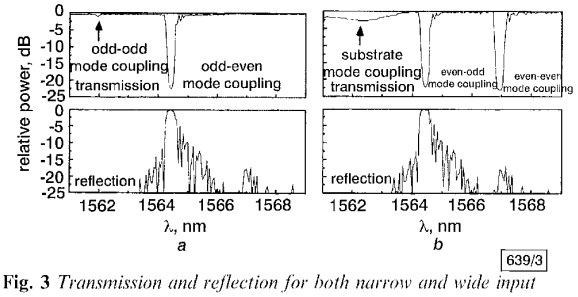

639/3

Fig. 3 *Transmission and reflection for both narrow and wide input*

a Narrow input
b Wide input

Typical performance is shown in Fig. 3. Both outputs show two sharp dips in transmission, although the second dip is very small for the narrow input. Dips of over 20 dB demonstrate excellent reflection. The sharp dip at the shorter wavelength for the wide input is at the same wavelength as the sharp dip at the longer wavelength for the narrow input. The grating equation and the operation of the device tell us that these dips are the even-odd and odd-even mode reflections that are wanted for add/drop filtering. The other sharp dips are unwanted even-even and odd-odd mode reflection. The broad dip at short wavelengths for the wide input is most likely coupling to substrate modes.

Looking at the reflection with the wide input, shown in Fig. 3*b*, these conclusions are confirmed. The peak corresponding to the sharp dip at the shorter wavelength peak is much larger. It is much more effectively 'dropped' out of the other port. The longer wavelength peak, even-even mode coupling, is almost non-existent as it is instead reflected back out the input port. It is possible to use the device effectively as an add/drop filter. Since the only critical function of the add and the drop ports is reflection out the other port, to the network it is insensitive to these unwanted dips. Using the wide input for adding/dropping, we are able to achieve the add/drop performance shown in Fig. 4. Extinction ratios of over 20 dB and 3 dB bandwidths of 0.4 nm (100 GHz) characterise the performance.

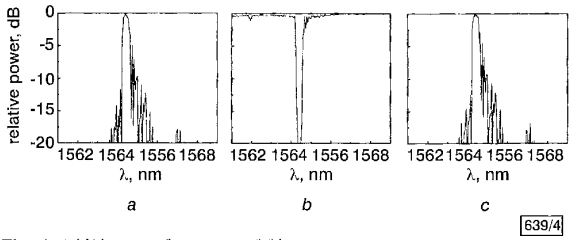

639/4

Fig. 4 *Add/drop performance of filter*

a Drop
b Pass
c Add

The presented data is all for TM polarisation. Looking in transmission at the odd-even mode dip of the narrow input, a polarisation dependence of ~0.25 nm is seen. Although this is unacceptable for a dense WDM component, it is a significant reduction from the 0.8 nm shift that has been characterised for surface ion-exchanged waveguide gratings [6]. This, combined with the results of [7], shows simply that the burial of the device was not sufficient enough for polarisation-independent operation. A deeper burial in the final step of the ion-exchanged waveguide process should allow us to reduce this shift to negligible amounts while not affecting the performance of the rest of the device.

In summary, we have demonstrated an add/drop filter using ion-exchange waveguide technology and photowritten Bragg gratings. The device exhibits 20 dB extinction ratios and 3 dB bandwidths of 0.4 nm (100 GHz), and a polarisation dependence of ~0.25 nm. Further improvement to the performance can be achieved by grating optimisation, a deeper burial step, and optimisation of the modes sensitivity to angular misalignment.

Acknowledgment: This work was done as BMDQ Phase I contract. The authors would like to acknowledge IOT for their partial support of this work.

1 December 2000
Electronics Letters Online No: 20010572
DOI: 10.1049/el:20010572

D.F. Geraghty, M. Morrell and S. Honkanen (*NP Photonis, UA Science and Technology Park, 9030 S. Rita Rd., Suite 120, Tucson, AZ 85747, USA*)

D. Provenzano and A. Yariv (*California Institute of Technology, Applied Physics Department, Mail Code 128-95, Pasadena, CA 91125, USA*)

N. Peyghambarian (*University of Arizona, Optical Sciences Center, 1630 E. University Blvd., Tucson, AZ 85721, USA*)

References

1 NAJAFI, S.I. (Ed.): 'Introduction to glass integrated optics' (Artech House, Norwood, MA, 1992)

2 ÄYRÄS, P., NUNZI CONTI, G., HONKANEN, S., and PEYGHAMBARIAN, N.: 'Birefringence control for ion-exchanged channel glass waveguides', *Appl. Opt.*, 1998, **37**, (36), pp. 8400–8405

3 PROVENZANO, D., MARSHALL, W.K., YARIV, A., GERAGHTY, D.F., HONKANEN, S., and PEYGHAMBARIAN, N.: 'Gratings formation in BGG31 glass by UV exposure', *Electron. Lett.*, 1999, **35**, (16), pp. 1332–1334

4 KEWITSCH, A.S., RAKULJIC, G.A., WILLEMS, P.A., and YARIV, A.: 'All-fiber zero-insertion-loss add-drop filter for wavelength-division multiplexing', *Opt. Lett.*, 1998, **23**, (2), pp. 106–108

5 MADSEN, C.K., STRASSER, T.A., MILBRODT, M.A., HENRY, C.H., BRUCE, A.J., and DEMARCO, J.: 'Planar waveguide add/drop filter employing a mode-converting grating in an adiabatic coupler'. Integrated Photonics Research Tech. Dig., Victoria, BC, Canada, March 30-April 1 1998, pp. 102–104

6 GERAGHTY, D.F., PROVENZANO, D., MARSHALL, W.K., HONKANEN, S., YARIV, A., and PEYGHAMBARIAN, N.: 'Gratings photowritten in ion-exchanged glass channel waveguides', *Electron. Lett.*, 1999, **35**, (7), pp. 585–587

7 GERAGHTY, D.F., PROVENZANO, D., MORRELL, M., INGENHOFF, J., HONKANEN, S., YARIV, A., and PEYGHAMBARIAN, N.: 'Polarisation independent Bragg gratings in ion-exchanged glass channel waveguides', *Electron. Lett.*, 2000, **36**, (6), pp. 531–532

1.5 μm wavelength distributed reflector lasers with vertical grating

J. Wiedmann, K. Ebihara, H.C. Kim, B. Chen, M. Ohta, K. Matsui, S. Tamura, J.-I. Shim and S. Arai

A 1.5 μm wavelength distributed reflector laser, consisting of a distributed Bragg reflector rear facet and a distributed feedback region, was realised using deep-etching technology. A low threshold current of I_{th} = 12.4 mA and a high differential quantum efficiency of η_d = 42% from the front facet was achieved with a submode suppression ratio of 33 dB ($I = 2.4I_{th}$) for a fifth-order grating, 220 μm long and 6 μm wide device at room temperature.

Introduction: Distributed reflector (DR) type lasers are well known for their good performance, e.g. high differential quantum efficiency, low threshold current and stable singlemode operation [1]. Previously, the fabrication of these devices required several epitaxial, lithographic and etching steps and was therefore time consuming and expensive. Progress in deep etching technology has overcome these drawbacks and reduced the required processing steps. Deep etching of fine structures was successfully performed vertically through the active region with high surface quality and little damage for photonic crystals, microdisk lasers and etched microcavities using reactive ion-beam etching (RIBE), reactive ion etching (RIE) or induction coupled plasma etching (ICPE). In previous work, lasers with deeply etched distributed Bragg reflector (DBR) facets having a high reflectivity were reported [2 – 4]. Singlemode operation was achieved by combining a DBR facet with coupled cavities [5] or ridge-type lasers with lateral gratings [6, 7].

In this Letter, we propose and successfully implement a vertically aligned grating, leading to a new type of DR laser. The schematic diagram and SEM photograph of this laser are shown in Fig. 1. The classical DR laser consists of regions with different gratings along the cavity, in which one region has high reflectivity. In the new design, a high-reflectivity DBR facet and a vertical grating form these different regions. Since the reflectivity bandwidth of the DBR is very broad (approximately 200 nm), matching the wavelengths of the corresponding regions can be accomplished easily.

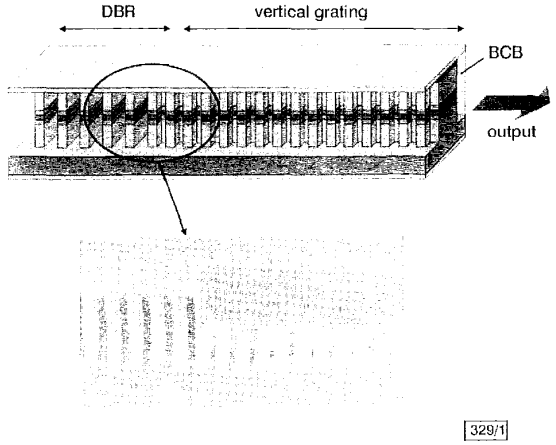

Fig. 1 *Schematic diagram and SEM photograph of DR laser consisting of DBR and vertical grating*

SEM photograph shows structure after dry etching and before coating with BCB

Modelling: The mesa width is denoted by W_S, its variation by ΔW_S and the grating period by Λ, as shown in Fig. 1. The light output is measured from the front right facet. The mesa is approximated by a slab waveguide consisting of the polymer benzocyclobutene (BCB, n = 1.546) as cladding and semiconductor material (n = 3.20) as the core. The equivalent refractive indices of the fundamental modes for the wide and narrow mesa widths of the grating sections are calculated. The coupling coefficient κ_i is estimated from the equivalent refractive index difference Δn_{eq} by $\kappa_i = 2\Delta n_{eq}/\lambda_B$ for a rectangular grating, where λ_B is the Bragg wavelength. The dependence of the coupling coefficient on the mesa width variation for various mesa widths is shown in Fig. 2. The coupling coefficient increases with increasing mesa width variation and is higher for narrower mesa widths.

Other issues, such as higher-order lateral mode propagation, higher surface recombination of the grating due to a larger surface area and increased damage due to dry etching, must be addressed in the analysis of the vertical grating. Furthermore, not only index coupling but also gain coupling mechanisms are present. Therefore, a more detailed theoretical and experimental study, which will be presented elsewhere, is required.

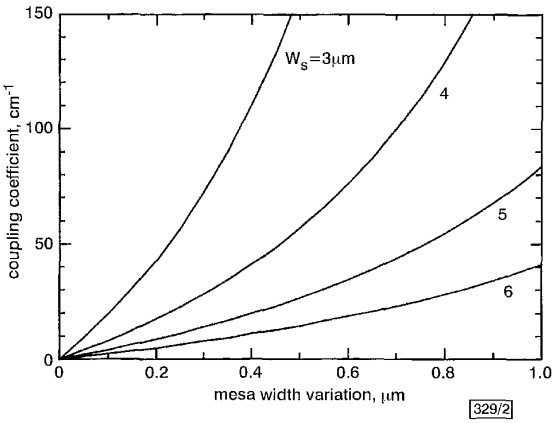

Fig. 2 *Estimation of coupling coefficient dependence on mesa width variation for various widths*

Fabrication: The vertical structure was grown by low-pressure organo-metallic vapour phase epitaxy LP-OMVPE on an n-InP substrate. After an n-InP buffer layer (1.5 μm thick, $N_D = 10^{18}$ cm^{-3}) was grown, GaInAsP lower and upper four-step OCLs (each step 29 nm thick, λ_g = 1.00, 1.05, 1.10 and 1.15 μm, respectively), the active region, consisting of five 1% compressively strained GaInAsP QWs (7 nm thick) and six –0.3% tensile strained barrier layers (9 nm thick, λ_g = 1.20 μm) were grown. A p-InP cladding layer (2.3 μm thick, $N_A = 5 \times 10^{17}$ cm^{-3}) and a p^+-GaInAs contact layer (300 nm thick, $N_A > 5 \times 10^{18}$ cm^{-3}) completed the structure.

The patterns, including the cavity with the grating and the DBR facet, were drawn by EB lithography using an 800 nm thick PMMA as the resist. Then Ti (80 nm thick) was deposited using an electron gun, and the mask was transferred by lift-off. Dry etching was performed in 15 alternating cycles of CH_4/H_2 RIE (CH_4:H_2 = 1:4, 6.5 Pa, RF power: 200 W, 5 min) and O_2 ashing (10 Pa, 50 W, 5 min) until an etching depth of 3.6 μm was obtained. After a wet chemical treatment, the polymer BCB was coated and baked in an N_2 atmosphere. The polymer BCB was used to protect and to passivate the structure [4, 5]. BCB was removed from the top of the mesa using CF_4/O_2 RIE. A Cr/Au contact was deposited on the top-side, the sample was thinned, and a Cr/Au contact was fabricated on the back.

Lasing properties: In previous research, deeply etched DBR lasers with a mesa width of W_S = 5 μm were fabricated [4]. We chose a mesa width of W_S = 6 μm and mesa width variation of ΔW_S = 0.5 μm so that similar conditions of the fabrication process could be used and lasing properties could be easily compared with those of the previous DBR lasers. The DBR region consists of 15 reflectors with a gap width of $3\lambda/(4n)$, a semiconductor length of $5\lambda/(4n)$ and a grating of the fifth order (Λ = 1200 nm). The front facet was cleaved and the laser was clip-mounted on to a small copper